

# WiT: Waypoint Diffusion Transformers via Trajectory Conflict Navigation

Hainuo Wang<sup>1\*</sup>, Mingjia Li<sup>1\*</sup>, and Xiaojie Guo<sup>1†</sup>

College of Intelligence and Computing, Tianjin University, Tianjin 300350, China  
{hainuo, mingjiali}@tju.edu.cn, xj.max.guo@gmail.com

**Abstract.** While recent Flow Matching models avoid the reconstruction bottlenecks of latent autoencoders by operating directly in pixel space, the lack of semantic continuity in the pixel manifold severely intertwines optimal transport paths. This induces severe *trajectory conflicts* near intersections, yielding sub-optimal solutions. Rather than bypassing this issue via information-lossy latent representations, we directly untangle the pixel-space trajectories by proposing **Waypoint Diffusion Transformers (WiT)**. WiT factorizes the continuous vector field via intermediate semantic waypoints projected from pre-trained vision models. It effectively disentangles the generation trajectories by breaking the optimal transport into prior-to-waypoint and waypoint-to-pixel segments. Specifically, during the iterative denoising process, a lightweight generator dynamically infers these intermediate waypoints from the current noisy state. They then continuously condition the primary diffusion transformer via the Just-Pixel AdaLN mechanism, steering the evolution towards the next state, ultimately yielding the final RGB pixels. Evaluated on ImageNet  $256 \times 256$ , WiT beats strong pixel-space baselines, accelerating JiT training convergence by  $2.2\times$ . Code will be publicly released at here.

**Keywords:** Image Generation · Flow Matching · Trajectory Conflict

## 1 Introduction

Diffusion models [12, 37], particularly those formalized through Flow Matching (FM) frameworks [1, 24, 25] and scaled via Diffusion Transformers (DiT) [26, 30], have established a new standard in highly realistic image generation. To mitigate the computational costs, these architectures traditionally operate in latent spaces [4, 31, 34], relying on continuous-valued variational autoencoders (VAEs) [10, 28, 31, 41] to compress raw visual signals. However, this two-stage design inherently introduces an information bottleneck. Consequently, visual tokenizers inevitably discard high-frequency textural details and frequently produce visual artifacts, placing a strict upper bound on overall generation quality [42]. To overcome these limitations, a recent paradigm shift, exemplified by architectures such as JiT [22], advocates for learning continuous vector fields directly in

---

\* Equal contribution.

† Corresponding author.

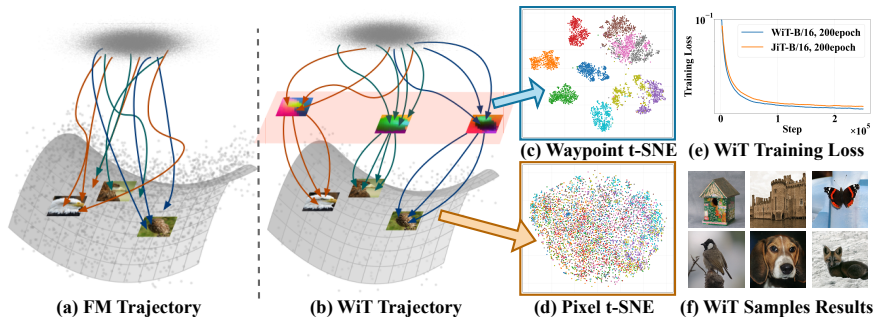


**Fig. 1:** An overview of our Waypoint Diffusion Transformers. (a) and (b) demonstrate the difference in trajectories before/after the waypoint is introduced. In standard pixel-space FM (a), mapping directly to an entangled, non-discriminative pixel manifold (d) induces severe trajectory conflict. With the integration of discriminative semantic waypoints (c), our WiT successfully converts the noise-to-pixel task into two stable, decoupled mappings. By routing the transport path, the generative flow is disentangled, thus mitigating path overlap. Consequently, WiT significantly accelerates convergence compared to baseline (e) while yielding highly realistic generated samples (f).

the original pixel space [6, 19, 27, 44]. By entirely bypassing the visual tokenizer, pixel-space Flow Matching eliminates compression-induced artifacts, offering a direct and theoretically lossless path for preserving fine-grained visual details.

Despite its simplicity, mapping directly from a shared noise distribution to a highly complex, multi-channel pixel distribution presents a formidable optimization challenge, as recent studies suggest that generative models inherently struggle to learn unconstrained, high-dimensional spaces from scratch [3, 42]. In the realm of latent diffusion, VA-VAE [42] addresses this optimization dilemma by aligning the VAE’s latent space with pre-trained vision foundation models. This alignment effectively regularizes the target manifold, rendering it more structured, uniform, and semantically discriminative. However, pure pixel-space generation operates under different constraints. Our target manifold (raw pixels) is naturally entangled and inherently non-discriminative (Figure 1(d)). Unlike learnable latent spaces, the pixel domain is locked to universal display standards and cannot be artificially reshaped to disentangle semantics. Consequently, standard pixel-space Flow Matching suffers from severe trajectory conflict [24, 25]. Transportation paths destined for visually similar but semantically distinct endpoints lack natural geometric separation, routinely converging in dense local regions of the noise space. Forced to minimize regression loss over overlapping paths, the neural network predicts an averaged velocity field [38]. This manifests as semantic bleeding and slower convergence. Techniques like Classifier-Free Guidance (CFG) [13] dynamically extrapolate the velocity logits using the difference between conditional and unconditional scores. While CFG effectively amplifies class-specific signal magnitudes, it is a post-hoc intervention that does not untangle the underlying spatial overlap of the training trajectories. A question naturally arises: *How can we provide clear, semantically separable guidance to a pixel-space vector flow without reverting to black-box latent spaces?*

Recognizing that the target pixel space is inherently non-discriminative and resistant to direct regularization, in this paper, we introduce a highly discriminative intermediate waypoint into the generative flow. We propose to explicitly decouple semantic navigation from pixel-level texture generation by reformulating the standard, unconstrained generative trajectory. Specifically, we decompose the challenging mapping between two non-discriminative manifolds (from the isotropic noise prior to the raw pixel distribution) by routing the transport path through a discriminative waypoint. Since the flow tradictory is bijective, this establishes two mathematically stable mappings: an initial mapping from the non-discriminative noise to the discriminative waypoint, followed by a mapping from this discriminative waypoint to the non-discriminative image space. By structuring the continuous vector field around these waypoints, we prevent the flow from collapsing into averaged, conflicting paths. This bipartite regularization not only mitigates severe trajectory conflict but also accelerates training convergence. To construct these robust semantic anchors, we leverage the feature spaces of modern self-supervised vision models [29, 35], exploiting their discriminative ability to ground visual subjects within the generative flow.

We implement this concept with WiT (**W**aypoints **D**iffusion **T**ransformers), a framework specifically designed to mitigate trajectory conflict in pixel-space Flow Matching. Instead of directly utilizing raw, high-dimensional representations from frozen vision foundation models, we apply Principal Component Analysis (PCA) to project these features onto a compact, low-dimensional semantic manifold. This relieves the burden of significant spatial redundancy and imposes a severe regression burden. By capturing only the principal directions of semantic variance, we extracted discriminative structural cues. Second, we integrate a lightweight waypoint generator into the flow matching pipeline, which is now optimized to reliably infer this condensed semantic waypoint from the noisy distribution at any integration timestep  $t$ . Finally, we design the pixel diffusion transformer to be spatially conditioned on these predicted semantic maps via our proposed Just-Pixel AdaLN mechanism. As the noisy state  $z_t$  evolves, the semantic guidance is naturally and continuously recalibrated, providing a rectifying force that steers the trajectory toward the correct class manifold and away from conflicting zones. As a result, WiT establishes a more effective architecture for pixel-space flow matching. Evaluations on ImageNet  $256 \times 256$  [7] generation demonstrate that our approach achieves superior boundary clarity and structural consistency compared to previous pixel-based baselines like JiT [22]. Our main contributions can be summarized as follows:

- We propose the Waypoint Diffusion Transformers (WiT), a novel generative paradigm that mitigates severe trajectory conflict in pixel-space Flow Matching. By anchoring flow trajectories to low-dimensional semantic manifolds, we introduce a decoupled pipeline that isolates semantic navigation from pixel-level generation.
- We introduce the Just-Pixel AdaLN mechanism. Unlike standard global conditioning, it leverages dynamically predicted semantic waypoints to provide spatially-varying modulation, ensuring semantic guidance.

- Through extensive experiments on ImageNet  $256 \times 256$ , WiT achieves state-of-the-art performance among purely pixel-space models. Crucially, explicit semantic grounding yields a  $2.2 \times$  training speedup compared with JiT-L/16.

## 2 Related Work

*Diffusion Models and Flow Matching.* Score-based diffusion models [12, 37] and their continuous-time ODE formulations have established a new paradigm for generative modeling. Early formulations learn a reversed stochastic process by predicting the injected noise (*i.e.*,  $\epsilon$ -prediction) [12]. Subsequent research revealed that shifting the prediction target to a noised quantity, such as the flow velocity ( $v$ -prediction) [32], could alter the optimization landscape and improve generation stability. More recently, Flow Matching [1, 24, 25] has unified these continuous-time processes into a simpler optimal transport framework. By explicitly formulating the mapping between a simple base and the target distribution, FM yields straightened probability flow ODE trajectories, leading to a reduction in steps. Concurrently, the backbone has undergone a significant transition. Diffusion Transformers [30] and Scalable Interpolant Transformers [26] have demonstrated that self-attention can effectively replace traditional dense U-Nets. Building upon these foundations, WiT aims to resolve the optimization instabilities in integrating complex, high-dimensional continuous vector fields.

*Generative Modeling in Pixel Space.* Generative Adversarial Networks [11, 33] and early Normalizing Flows [9, 17] operate directly in the raw pixel space. However, scaling these early pixel-based approaches to high-resolution synthesis proved computationally prohibitive. Thus, the field experienced a paradigm shift toward latent-space modeling, propelled by VQ-VAE [10] and LDM [31]. These methods compress high-dimensional images into low-dimensional latent manifolds before generation. While this latent compression mitigates computational bottlenecks, it is inherently lossy; it inevitably introduces information bottlenecks, spatial reconstruction artifacts, and a noticeable degradation of textural details. In pursuit of a high-fidelity generation, a recent shift advocates for pure pixel-space modeling [6, 19, 27, 44]. Advances such as SiD2 [15], and PixelFlow [5] demonstrate that scalable large-patch Vision Transformers can now directly model raw pixels without relying on auxiliary tokenizers. However, directly operating in this high-dimensional domain introduces a new bottleneck: according to the manifold assumption, while clean data lies on a low-dimensional manifold, intermediate noisy states inherently span the full high-dimensional space. JiT [22] attempts to mitigate this by  $x$ -prediction. However, mapping a highly complex pixel distribution directly from noise severely exacerbates the overlapping of trajectories. WiT embraces the pure pixel-space paradigm but proposes a reorganization to bypass these high-dimensional ambiguities.

*Mitigating Optimization Conflict via Representation Alignment.* In the conditional Flow Matching regime, we use the neural network to estimate a unified

vector field that transports shared Gaussian noise to thousands of distinct semantic classes simultaneously. Since pixel space is semantically entangled, paths destined for visually similar but semantically distinct endpoints lack natural geometric separation. During intermediate integration phases, these class-conditional optimal transport paths routinely converge or cross. As recently formalized by the optimization dilemma [42], this forces the neural network to minimize the regression loss by predicting an averaged velocity field. Recent literature has also begun exploring the intersection of representation learning and generative diffusion. Methods like REPA [43], REPA-E [20, 21], iREPA [36], and RAE [45] attempt to align the internal representations of diffusion transformers with pre-trained representation encoders to accelerate convergence. However, these prior methods typically operate within heavily compressed latent spaces or treat representations merely as auxiliary loss supervisions. In stark contrast, WiT explicitly constructs low-dimensional semantic waypoints derived dynamically from these representations and trains a dedicated, lightweight Waypoints DiT to navigate toward them. More importantly, through our proposed Just-Pixel AdaLN mechanism, these predicted waypoints serve as dense, spatially varying conditions that structurally anchor the massive Pixel Space DiT.

### 3 Methodology

In this section, we detail the formulation and architecture of the proposed Waypoint Diffusion Transformers (WiT). We first review the standard pixel-space Flow Matching framework and formalize the trajectory conflict. To resolve these ambiguities, we introduce the construction of low-dimensional semantic waypoints derived from pre-trained vision models. Finally, as illustrated in Figure 2, we present our WiT, detailing how the proposed Just-Pixel AdaLN mechanism modulates the transformer features with spatially-varying semantic guidance, explicitly decoupling semantic navigation from high-realistic pixel generation.

#### 3.1 Pixel-Space Flow Matching and Trajectory Conflict

Following standard Flow Matching frameworks, let  $x \in \mathbb{R}^{H \times W \times 3}$  denote a clean target image, and  $\epsilon \sim \mathcal{N}(0, \mathbf{I})$  denote standard Gaussian noise. The intermediate noisy state  $z_t$  at timestep  $t \in [0, 1]$  is defined as  $z_t = tx + (1 - t)\epsilon$ .

The ground-truth velocity vector field driving the state from noise to data is mathematically given by  $v = x - \epsilon$ . As exemplified by state-of-the-art pixel models like JiT [22],  $x$ -prediction is recommended for pixel space generation, *i.e.*, training a parameterized network  $G_\theta$  to predict the clean image  $\hat{x}$  directly. From this, the estimated velocity is analytically constructed as:

$$\hat{v} = \frac{\hat{x} - z_t}{1 - t}. \quad (1)$$

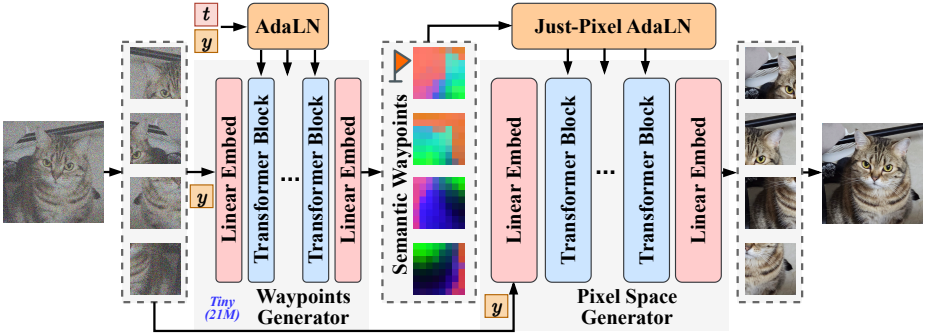


**Fig. 2:** Overview of the WiT architecture. *Left:* A lightweight Waypoints Generator (21M params) predicts Semantic Waypoints from the noisy state  $z_t$ . *Right:* The Pixel Space Generator synthesizes the image, utilizing these predicted waypoints as spatial conditions via the Just-Pixel AdaLN mechanism.

The network is then optimized using a velocity-matching objective ( $v$ -loss), which aligns the estimated velocity with the ground-truth vector field:

$$\mathcal{L}_v = \mathbb{E}_{x,\epsilon,t,y} \left[ \|\hat{v} - v\|_2^2 \right] = \mathbb{E}_{x,\epsilon,t,y} \left[ \left\| \frac{\hat{x} - z_t}{1-t} - (x - \epsilon) \right\|_2^2 \right]. \quad (2)$$

However, mapping directly from a class-agnostic Gaussian prior to a complex pixel distribution under this objective incurs severe trajectory conflict. Under the MSE objective, the optimal denoiser  $\hat{x}^*$  at any intermediate timestep  $t$  is the conditional expectation of the target data given the noisy observation:

$$\hat{x}^*(z_t) = \mathbb{E}[x|z_t]. \quad (3)$$

The trajectory conflict can be formalized as the irreducible variance of this optimal estimator. Because the pixel space is semantically highly entangled, diverse target images  $x$  corresponding to radically different semantic classes share identical dense neighborhoods in the input noise space as  $t \rightarrow 0$ . This ambiguity at coordinate  $z_t$  can be quantified by the variance of the target distribution:

$$\text{Var}(x|z_t) = \mathbb{E} \left[ \|x - \mathbb{E}[x|z_t]\|_2^2 \mid z_t \right]. \quad (4)$$

Attempting to blindly regress divergent endpoints  $x$  from overlapping initial states yields an extremely large  $\text{Var}(x|z_t)$ . To minimize the regression loss, the neural network is forced to output the averaged state  $\mathbb{E}[x|z_t]$ , causing severe gradient interference and limiting convergence.

To resolve this, we hypothesize that explicit semantic grounding can partition the optimal vector field. By introducing a discriminative intermediate semantic waypoint  $s_0$ , the optimal predictor becomes conditioned on both the noisy state and the semantic topology:  $\hat{x}_{\text{WiT}}^*(z_t, s_0) = \mathbb{E}[x|z_t, s_0]$ . According to the Law of Total Variance, the original trajectory conflict is decomposed as:

$$\text{Var}(x|z_t) = \mathbb{E}_{s_0} [\text{Var}(x|z_t, s_0)] + \text{Var}_{s_0} (\mathbb{E}[x|z_t, s_0]). \quad (5)$$

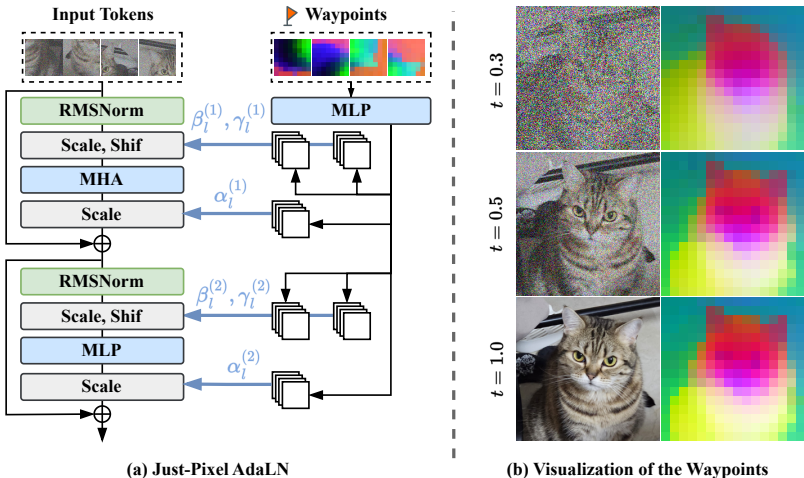


**Fig. 3:** (a) Just-Pixel AdaLN: The predicted semantic waypoints provide spatially varying modulation. (b) Visualization of the predicted semantic waypoints and intermediate pixel states during inference. *Left.* The evolving noisy pixel states  $z_t$  at different integration timesteps. *Right.* The corresponding spatial semantic waypoints  $\hat{s}_0$  dynamically inferred by our lightweight Waypoints Generator.

In our decoupled architecture, the variance component  $\text{Var}_{s_0}(\mathbb{E}[x|z_t, s_0])$  is explicitly resolved by predicting  $s_0$ . As recently formalized by VA-VAE [42], mapping continuous flows from an isotropic noise prior to a highly discriminative, low-dimensional space is inherently more tractable and avoids severe gradient interference. Consequently, the primary pixel generator is only tasked with resolving the residual variance  $\text{Var}(x|z_t, s_0)$ . Because the semantic waypoint  $s_0$  tightly bounds the target manifold to a specific affine subspace, this residual variance is substantially smaller than the unconditioned total variance  $\text{Var}(x|z_t)$ . By firmly anchoring the vector field to these semantic guides, generative trajectories are steered to bypass overlapping zones. More details can be found in Section 5.

### 3.2 Constructing Semantic Waypoints

To eliminate the geometric ambiguity of intersecting trajectories, the generative process must be firmly anchored by an intermediate structural guide. We leverage the highly separable representation space of frozen self-supervised vision models, specifically DINOv3 [35], to serve as these ground-truth semantic anchors.

For a given target image  $x$ , we extract dense, patch-wise semantic tokens  $\phi(x) \in \mathbb{R}^{N \times D}$ . Because raw DINOv3 features possess a high dimensionality that imposes a severe optimization burden, we construct a compact affine subspace via Principal Component Analysis fitted on the training distribution. Let  $U_d \in \mathbb{R}^{D \times d}$  denote the projection matrix for the top  $d = 64$  principal components, and  $\mu$  be the dataset mean. We define the explicit ground-truth semantic waypoint  $s_0$  as:

$$s_0 = (\phi(x) - \mu)U_d \in \mathbb{R}^{N \times 64}. \quad (6)$$

This orthogonal projection constructs a low-dimensional manifold optimized for class separability. By exploiting the intrinsic sparsity and low-rank structure of these feature spaces, we establish a tractable optimization landscape that acts as a direct, structural supervisory signal for our framework.

*Lightweight Waypoints Generator.* We introduce a lightweight transformer, denoted as  $W_\psi$ , which operates on the pixel-level noisy observation  $z_t = tx + (1-t)\epsilon_{\text{img}}$ . Conditioned on the timestep  $t$  and class label  $y$  via standard AdaLN,  $W_\psi$  is tasked with resolving the clean semantic waypoint  $\hat{s}_0 = W_\psi(z_t, t, y)$  from the high-dimensional pixel noise. To supervise this cross-domain mapping, we establish a parallel probability flow ODE in the semantic space. Let  $z_{\text{sem},t} = ts_0 + (1-t)\epsilon_{\text{sem}}$  denote the intermediate state on the semantic trajectory, constructed with an independent Gaussian noise  $\epsilon_{\text{sem}} \sim \mathcal{N}(0, \mathbf{I})$ . The objective is to match the analytically derived semantic velocity  $\hat{v}_{\text{sem}} = (\hat{s}_0 - z_{\text{sem},t}) / \max(1-t, \tau_{\text{eps}})$  with the target ground-truth velocity  $v_{\text{sem}} = (s_0 - z_{\text{sem},t}) / \max(1-t, \tau_{\text{eps}})$ . The generator minimizes the following loss:

$$\mathcal{L}_{\text{sem}} = \mathbb{E}_{x, s_0, \epsilon_{\text{img}}, \epsilon_{\text{sem}}, t, y} \left[ \left\| \frac{\hat{s}_0 - z_{\text{sem},t}}{\max(1-t, \tau_{\text{eps}})} - \frac{s_0 - z_{\text{sem},t}}{\max(1-t, \tau_{\text{eps}})} \right\|_2^2 \right], \quad (7)$$

where  $\tau_{\text{eps}}$  denotes a small positive constant introduced to prevent numerical instability (*i.e.*, division by zero) as  $t \rightarrow 1$ . Given its highly compressed target dimension ( $d = 64$ ),  $W_\psi$  requires minimal capacity (*e.g.*, 21M parameters) and serves as an efficient navigator for the primary diffusion process.

### 3.3 Semantic-Pixel Decoupled Architecture

Rather than enforcing a direct, unconstrained mapping from noise to raw pixels, WiT decomposes the generative process into a decoupled architecture. As shown in Figure 2, the framework consists of a lightweight Waypoints Generator and a primary Pixel Space Generator.

*Pixel Space Generator via Just-Pixel AdaLN.* Once the semantic waypoint  $\hat{s}_0$  is inferred, it is injected into the primary Pixel Space Generator  $G_\theta$ . To disentangle the semantic waypoint from pixel-space generation, we propose the Just-Pixel AdaLN mechanism. As shown in Figure 3 (a), unlike standard AdaLN, which modulates tokens uniformly via a globally pooled time-class embedding  $e(t, y)$ , our mechanism provides spatially-varying guidance. We aggregate the global conditioning and the localized semantic map into a unified spatial condition  $c_s = e(t, y) + \text{Proj}(\hat{s}_0)$ , where  $\text{Proj}(\cdot)$  is a linear projection mapping the 64-dimensional sequence to the transformer’s hidden dimension  $D_h$ . For the  $l$ -th transformer block, given the hidden token sequence  $h_l \in \mathbb{R}^{N \times D_h}$ , the condition

**Algorithm 1** Training Procedure of WiT

**Require:** Dataset  $\mathcal{D}$ , Pre-trained model  $\phi$ , PCA projection  $U_d$ , dataset mean  $\mu$

**Require:** Waypoints Generator  $W_\psi$ , Pixel Space Generator  $G_\theta$

- 1: **Training the Waypoints Generator**
- 2: **while**  $W_\psi$  has not converged **do**
- 3:   Sample  $(x, y) \sim \mathcal{D}$ ,  $t \sim \mathcal{U}[0, 1]$ , and  $\epsilon_{\text{img}}, \epsilon_{\text{sem}} \sim \mathcal{N}(0, \mathbf{I})$
- 4:    $s_0 \leftarrow (\phi(x) - \mu)U_d$                                // Extract ground-truth semantic waypoint
- 5:    $z_t \leftarrow tx + (1 - t)\epsilon_{\text{img}}$                                // Construct noisy pixel state
- 6:    $z_{\text{sem}, t} \leftarrow ts_0 + (1 - t)\epsilon_{\text{sem}}$                                // Construct noisy semantic state
- 7:    $\hat{s}_0 \leftarrow W_\psi(z_t, t, y)$                                // Predict clean waypoint from pixel noise
- 8:    $\mathcal{L}_{\text{sem}} \leftarrow \left\| \frac{\hat{s}_0 - z_{\text{sem}, t}}{\max(1-t, \tau_{\text{eps}})} - \frac{s_0 - z_{\text{sem}, t}}{\max(1-t, \tau_{\text{eps}})} \right\|_2^2$
- 9:   Update  $\psi$  via gradient descent on  $\mathcal{L}_{\text{sem}}$
- 10: **end while**
- 11: **Training the Pixel Space Generator**
- 12: Freeze the trained Waypoints Generator  $W_\psi$
- 13: **while**  $G_\theta$  has not converged **do**
- 14:   Sample  $(x, y) \sim \mathcal{D}$ ,  $t \sim \mathcal{U}[0, 1]$ , and  $\epsilon_{\text{img}} \sim \mathcal{N}(0, \mathbf{I})$
- 15:    $z_t \leftarrow tx + (1 - t)\epsilon_{\text{img}}$                                // Construct noisy pixel state
- 16:    $\hat{s}_0 \leftarrow W_\psi(z_t, t, y)$                                // Infer semantic condition via frozen  $W_\psi$
- 17:    $\hat{x} \leftarrow G_\theta(z_t, t, y, \hat{s}_0)$                                // Spatially-conditioned pixel generation
- 18:    $\mathcal{L}_{\text{img}} \leftarrow \left\| \frac{\hat{x} - z_t}{1-t} - (x - \epsilon_{\text{img}}) \right\|_2^2$
- 19:   Update  $\theta$  via gradient descent on  $\mathcal{L}_{\text{img}}$
- 20: **end while**

$c_s$  is projected into six spatially-varying modulation parameters to govern both the self-attention and MLP mechanisms:

$$\gamma_l^{(1)}, \beta_l^{(1)}, \alpha_l^{(1)}, \gamma_l^{(2)}, \beta_l^{(2)}, \alpha_l^{(2)} = \text{Linear}_l(c_s). \quad (8)$$

Following the AdaLN-Zero formulation, these continuous spatial maps sequentially modulate the normalized features and gate the residual connections:

$$\tilde{h}_l = h_l + \alpha_l^{(1)} \odot \text{Attention}((1 + \gamma_l^{(1)}) \odot \text{RMSNorm}(h_l) + \beta_l^{(1)}), \quad (9)$$

$$h_{l+1} = \tilde{h}_l + \alpha_l^{(2)} \odot \text{MLP}((1 + \gamma_l^{(2)}) \odot \text{RMSNorm}(\tilde{h}_l) + \beta_l^{(2)}). \quad (10)$$

By delegating semantic navigation to the waypoints generator, Just-Pixel AdaLN allows the primary transformer to focus entirely on high-realistic spatial generation. Finally,  $G_\theta$  minimizes the pixel-level velocity-matching objective:

$$\mathcal{L}_{\text{img}} = \mathbb{E}_{x, \epsilon_{\text{img}}, t, y} \left[ \left\| \frac{\hat{x} - z_t}{1-t} - (x - \epsilon_{\text{img}}) \right\|_2^2 \right]. \quad (11)$$

By explicitly grounding the pixel-level velocity field in a tractable semantic manifold, our WiT significantly enhances optimization stability and spatial realistic without relying on autoencoder-based latent compression. As summarized



**Table 1:** Configuration of Experiments for WiT.

|                               | WiT-B | WiT-L   | WiT-XL |
|-------------------------------|-------|---|--------|
| <b>Architecture</b>           |       |   |        |
| depth                         | 12    | 24  | 28     |
| hidden dim                    | 768   | 1024  | 1152   |
| heads                         | 12    | 16  | 16     |
| image size                    |       | 256   |        |
| patch size                    |       | 16  |        |
| bottleneck                    |       | 128   |        |
| dropout                       |       | 0   |        |
| <b>Training</b>               |       |   |        |
| epochs                        |       | 200 (ablation), 600   |        |
| warmup epochs                 |       | 5   |        |
| optimizer                     |       | AdamW, $\beta_1 = 0.9, \beta_2 = 0.95$                                      |        |
| batch size                    |       | 1024  |        |
| learning rate                 |       | $5 \times 10^{-5}$  |        |
| learning rate schedule        |       | constant  |        |
| weight decay                  |       | 0   |        |
| ema decay                     |       | {0.9996, 0.9999}  |        |
| time sampler                  |       | $\text{logit}(t) \sim \mathcal{N}(\mu, \sigma^2), \mu = -0.8, \sigma = 0.8$ |        |
| noise scale                   |       | $1.0 \times \text{image\_size}/256$   |        |
| clip of $(1 - t)$ in division |       | 0.05  |        |
| class token drop (for CFG)    |       | 0.1   |        |
| <b>Sampling</b>               |       |   |        |
| ODE solver                    |       | Heun  |        |
| ODE steps                     |       | 50  |        |
| time steps                    |       | linear in $[0.0, 1.0]$  |        |
| CFG scale sweep range         |       | $[1.0, 4.0]$  |        |
| CFG interval [18]             |       | $[0.1, 1.0]$ (if used)  |        |

to compute the PCA projection matrix, compressing the raw DINOv3 features to a compact dimension of  $d = 64$ . During the training stage, the Waypoints Generator  $W_\psi$  is first optimized for 600 epochs to master semantic velocity matching on the PCA-reduced DINOv3 features. The Pixel Space Generator  $G_\theta$  is then trained for up to 600 epochs, conditioned on the frozen Exponential Moving Average weights of  $W_\psi$ . We utilize the AdamW optimizer with a constant learning rate schedule, a base learning rate of  $5 \times 10^{-5}$ , and a 5-epoch linear warmup.

To facilitate reproducibility and provide a comprehensive overview of our architectural scaling, Table 1 details the exact hyperparameter configurations for the Waypoint Diffusion Transformers (WiT) across three capacity scales: Base (B), Large (L), and Extra-Large (XL).

In addition, several critical low-level mechanisms are implemented to ensure the stability of pure pixel-space Flow Matching following JiT [22]. First, we adopt a logit-normal distribution ( $\mu = -0.8, \sigma = 0.8$ ) for sampling the integra-

**Table 2:** Comprehensive comparison of class-conditional ImageNet  $256 \times 256$ .

| Method                                    | Params   | Epochs | IS $\uparrow$ | FID-50K $\downarrow$ |
|---|----------|--------|---------------|----------------------|
| <i>Latent-space Diffusion Models</i>      |          |        |               |                      |
| DiT-XL/2 [30]                             | 675+49M  | -      | 278.2         | 2.27                 |
| SiT-XL/2 [26]                             | 675+49M  | -      | 277.5         | 2.06                 |
| REPA (SiT-XL/2) [43]                      | 675+49M  | -      | 305.7         | 1.42                 |
| LightningDiT-XL/2 [42]                    | 675+49M  | -      | 295.3         | 1.35                 |
| DDT-XL/2 [41]                             | 675+49M  | -      | 310.6         | 1.26                 |
| RAE (DiT <sup>DH</sup> -XL/2) [45]        | 839+415M | -      | 262.6         | <b>1.13</b>          |
| <i>Pixel-space Models (Non-diffusion)</i> |          |        |               |                      |
| JetFormer [39]                            | 2.8B     | -      | -             | 6.64                 |
| FractalMAR-H [23]                         | 848M     | -      | 348.9         | 6.15                 |
| <i>Pixel-space Diffusion Models</i>       |          |        |               |                      |
| ADM-G [8]                                 | 554M     | -      | 186.7         | 4.59                 |
| RIN [16]                                  | 410M     | -      | 182.0         | 3.42                 |
| SiD (UViT/2) [14]                         | 2B       | -      | 256.3         | 2.44                 |
| PixelFlow (XL/4) [5]                      | 677M     | -      | 282.1         | 1.98                 |
| PixNerd (XL/16) [40]                      | 700M     | -      | 297.0         | 2.15                 |
| JiT-H/16 [22]                             | 953M     | -      | 303.4         | 1.86                 |
| JiT-G/16 [22]                             | 2B       | -      | 292.6         | <b>1.82</b>          |
| LF-DiT-L/16 [2]                           | 465M     | 200    | -             | 2.48                 |
| <i>Direct Baselines &amp; Ours</i>        |          |        |               |                      |
| JiT-B/16 [22]                             | 131M     | 200    | -             | 4.37                 |
| <b>WiT-B/16 (Ours)</b>                    | 131M+21M | 200    | <b>270.7</b>  | <b>3.34</b>          |
| JiT-B/16 [22]                             | 131M     | 600    | 275.1         | 3.66                 |
| <b>WiT-B/16 (Ours)</b>                    | 131M+21M | 600    | <b>280.2</b>  | <b>3.03</b>          |
| JiT-L/16 [22]                             | 459M     | 200    | -             | 2.79                 |
| <b>WiT-L/16 (Ours)</b>                    | 459M+21M | 200    | <b>289.1</b>  | <b>2.38</b>          |
| JiT-L/16 [22]                             | 459M     | 600    | 298.5         | 2.36                 |
| <b>WiT-L/16 (Ours)</b>                    | 459M+21M | 265    | 293.7         | 2.36                 |
| <b>WiT-L/16 (Ours)</b>                    | 459M+21M | 600    | <b>303.3</b>  | <b>2.22</b>          |
| WiT-XL/16 (Ours)                          | 676M+21M | 200    | 292.3         | 2.16                 |
| <b>WiT-XL/16 (Ours)</b>                   | 676M+21M | 600    | <b>311.8</b>  | <b>2.09</b>          |

tion timestep  $t$  during training. This non-uniform sampling strategy deliberately concentrates the training capacity on intermediate noise levels, where the optimal transport paths are most entangled and the trajectory conflict is most severe. Second, to strictly prevent numerical explosion when computing the  $v$ -prediction loss as  $t \rightarrow 1$ , we enforce a clipping mechanism that bounds the denominator  $(1 - t)$  at a minimum threshold of 0.05. Finally, during the inference stage, we employ a truncated Classifier-Free Guidance (CFG) [13] strategy, parameterized by the *CFG interval* [18].

## 4.2 Main Results

*Quantitative Results.* We compare WiT against a comprehensive set of state-of-the-art generative models, including leading latent-space diffusion models (*e.g.*, DiT [30], SiT [26]), pixel-space non-diffusion models (*e.g.*, JetFormer [39]), and purely pixel-space diffusion models (*e.g.*, PixelFlow [5], PixNerd [40]), and our direct baseline JiT [22]). As shown in Table 2, WiT consistently outperforms



Fig. 4: Qualitative Results of WiT-L/16 on ImageNet  $256 \times 256$  [7].

its pixel-space counterparts at every comparable stage, highlighting massive improvements in training efficiency and sample realism.

With the B/16 configuration, WiT achieves an FID of 3.34 at just 200 epochs, already surpassing the vanilla JiT [22] trained for 600 epochs (3.66). Extending the training to 600 epochs, WiT reaches a superior FID of 3.03, demonstrating that explicit semantic waypoints significantly accelerate convergence and elevate the performance ceiling of pixel-space modeling. At the L/16 scale, WiT consistently outperforms both the pixel-space baseline (JiT [22]) and the Latent Forcing (LF-DiT [2]) under identical training budgets. With only 265 epochs of training, WiT achieves an FID of 2.36 and a high Inception Score of 293.7. Notably, this matches the performance of the JiT-L baseline at 600 epochs, delivering an impressive  $2.27\times$  training speedup. Crucially, when WiT-L/16 is extended to 600 epochs, it achieves an exceptional FID of 2.22 and an IS of 303.3. This milestone not only eclipses its pixel-space counterpart JiT-L/16 (2.36 FID), but also surpasses the heavy latent-space benchmark DiT-XL/2 (2.27 FID). Remarkably, WiT achieves these substantial performance leaps with the negligible computational overhead of a 21M waypoint generator. This confirms that anchoring the vector field in separable semantic manifolds allows pixel-space models to rival VAE-compressed latent models without relying on brute-force parameter scaling. Furthermore, the results demonstrate that our framework scales well with increased model capacity. By scaling the architecture to the Extra-Large (WiT-XL/16) configuration, the generative quality is further enhanced, peaking at an FID of 2.09 and an IS of 311.8 after 600 epochs. Notably, this remarkable

**Table 3:** Ablation studies on WiT-B/16 (200 epochs). We investigate the impact of semantic bottleneck size ( $d$ ) and the architectural injection method.

| Configuration                           | PCA ( $d$ ) | Injection               | IS $\uparrow$ | FID $\downarrow$ |
|---|-------------|-------------------------|---------------|------------------|
| <i>Ablation on Bottleneck Dimension</i> |             |                         |               |                  |
| WiT-B/16                                | 32          | Just-Pixel AdaLN        | 210.40        | 5.11             |
| WiT-B/16                                | 128         | Just-Pixel AdaLN        | 211.33        | 4.12             |
| <i>Ablation on Injection Mechanism</i>  |             |                         |               |                  |
| WiT-B/16                                | 64          | Channel Concat          | 221.19        | 3.93             |
| WiT-B/16                                | 64          | In-context Concat       | 238.92        | 3.63             |
| <b>WiT-B/16 (Ours)</b>                  | <b>64</b>   | <b>Just-Pixel AdaLN</b> | <b>270.73</b> | <b>3.34</b>      |

Inception Score surpasses many prominent latent-space diffusion models (*e.g.*, DiT-XL/2 [30], SiT-XL/2 [26], REPA (SiT-XL/2) [43], LightningDiT-XL/2 [42], DDT-XL/2 [41], RAE (DiT<sup>DH</sup>-XL/2) [45], to name just a few).

*Qualitative Results.* Figure 4 showcases highly realistic ImageNet  $256 \times 256$  samples generated by WiT-L/16, corroborating our quantitative leaps and highlighting two core advantages. First, WiT exhibits exceptional structural coherence. By utilizing dynamically predicted semantic waypoints as steadfast navigational anchors, animals and complex scenes (*e.g.*, the lion and castle) maintain correct proportions and strict perspectives, avoiding the severe geometric distortions typical of unanchored pixel-space models. Second, operating purely in pixel space preserves pristine, high-frequency micro-textures (*e.g.*, fine owl feathers and intricate butterfly wings) that are often corrupted by VAE-based latent compression. By marrying the structural stability of semantic representations with the uncompressed realism of raw pixels, WiT establishes a highly robust paradigm for photorealistic generation. Finally, to qualitatively demonstrate the structural integrity, visual realism, and diversity of our approach, we provide additional uncurated generated samples in Figure 6, 7, 8, 9, 10, 11, 12, 13.

### 4.3 Ablation Studies

To validate the effectiveness of WiT’s components and settings, we perform ablations on the semantic waypoint dimensionality, the feature injection mechanism, and the CFG scale during inference with WiT-B/16 under 200 epochs in Table 3.

*PCA Dimension  $d$ .* We evaluate the impact of the semantic waypoint’s information density by varying the number of PCA components  $d$ . The dimension  $d$  essentially dictates the trade-off between semantic expressiveness and optimization complexity. As shown in Table 3, using an excessively large dimension ( $d = 128$ ) exacerbates the curse of dimensionality. This makes the waypoint space unnecessarily complex, hindering the predictor’s ability to map smooth trajectories and converge optimally (sub-optimal FID of 4.12). Conversely, extreme compression ( $d = 32$ ) induces a severe information bottleneck. By inadvertently discarding vital structural variances, it results in semantic under-fitting; the waypoints lose

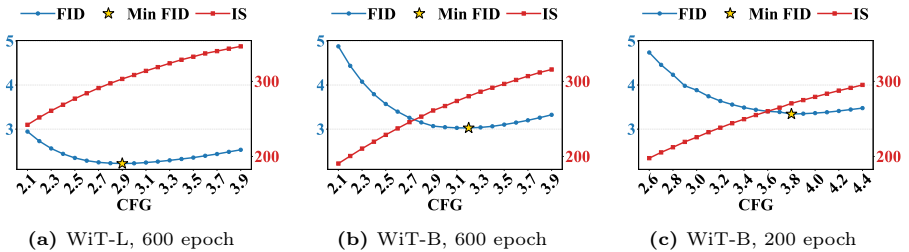


**Fig. 5:** The impact of CFG on FID and IS. The gold star indicates the minimum FID.

their discriminative power, causing a significant drop in sample quality (FID 5.11) as the network struggles to anchor onto distinct generative modes. We find that  $d = 64$  provides an optimal balance. At this dimension, the PCA projection filters out non-essential noise while strictly preserving the core structural topology. This ensures that the latent representations remain highly clusterable, providing dense and reliable semantic anchors for stable trajectory learning.

*Semantic Injection Strategy.* We compare three methods for grounding the Pixel Space Generator  $G_\theta$  with the predicted semantic waypoints: 1) Channel Concat: Concatenating  $\hat{s}_0$  directly to the input pixel noisy patches along the channel dimension; 2) In-context Concat: Appending semantic tokens as an in-context prefix to the Transformer sequence; 3) Just-Pixel AdaLN: Pure localized spatial modulation without invasive sequence concatenation. As reported in Table 3, Channel Concat performs the worst, resulting in an FID of 3.93 and an IS of 221.19. By forcibly fusing highly abstract semantic vectors with raw noisy pixels at the initial projection layer, it creates a representational mismatch that burdens the network’s early optimization. In-context Concat mitigates this mismatch by treating waypoints as separate prefix tokens, allowing the self-attention mechanism to query semantics dynamically. This improves the FID to 3.63 and the IS to 238.92. However, this invasive sequence extension still disrupts the native pixel-to-pixel attention manifold and forces the model to implicitly learn how to route prefix tokens to corresponding local spatial patches. In contrast, our Just-Pixel AdaLN achieves the best performance by a significant margin, securing the lowest FID of 3.34 and a substantially higher IS of 270.73. By injecting semantics through spatially varying affine modulations across intermediate transformer blocks, it avoids polluting the token sequence. This mechanism superiorly preserves the generative model’s internal attention priors while strictly and explicitly enforcing the localized semantic layout at every network depth.

*CFG Scale.* Finally, we investigate the impact of the CFG scale on generation quality across model capacities and training durations. As in Figure 5, we trace the FID and Inception Score for WiT-L (600 epochs), WiT-B (600 epochs), and WiT-B (200 epochs). Notably, it forms a distinct U-shaped curve, with the optimal point shifting depending on the model’s maturity. The fully trained WiT-L/16 model achieves its optimal FID at a low CFG scale of 2.9. WiT-B at

600 epochs peaks at a CFG of 3.1, while the early-stage WiT-B (200 epochs) relies on a much higher CFG of 3.8 to reach its minimum FID. This demonstrates that as our decoupled architecture is scaled up or trained longer, the model’s inherent semantic mapping capability becomes substantially stronger, thereby reducing the reliance on heavy CFG extrapolation.

## 5 Quantitative Analysis of Trajectory Conflict

Building upon the trajectory conflict formalized in Section 3.1, this section provides a theoretical motivation for search space contraction from a Bayes-risk perspective and empirically validates the reduced trajectory conflict.

The trajectory conflict in pure pixel-space generation stems from an excessively large and unconstrained search space. From a probabilistic perspective, WiT resolves this by introducing an explicit *semantic constraint*. Rather than modeling the highly entangled marginal distribution  $p(x|z_t)$  directly, we utilize the semantic prior to model the conditionally constrained distribution  $p(x, s_0|z_t)$ . Operationally, this is realized through the injection of intermediate semantic waypoints via our Just-Pixel AdaLN modulation. In terms of optimization, this structural constraint is explicitly enforced by our dual-loss formulation ( $\mathcal{L}_{\text{sem}}$  and  $\mathcal{L}_{\text{img}}$ ). By satisfying the semantic constraint first, the generative search space for the pixel flow is shrunk. This theoretical reduction in search space directly translates to our observed behavioral advantages, most notably highly stabilized optimal transport paths and a  $2.2\times$  acceleration in training convergence.

To theoretically formalize our claim that the semantic constraint drastically shrinks the generative search space, we can analyze the ambiguity of the denoising target at any noisy state  $z_t$  using the conditional variance of the target distribution. We first consider an oracle setting where the true semantic waypoint  $s_0$  is observed. In standard pixel-space  $x$ -prediction, the optimal denoiser network minimizes the Mean Squared Error (MSE) and converges to the conditional expectation:

$$\hat{x}^*(z_t) = \mathbb{E}_{x \sim p(x|z_t)}[x]. \quad (12)$$

The irreducible error of this optimal predictor represents the ambiguity without semantic conditioning, which is given by the trace of the conditional covariance matrix:

$$\mathcal{E}_{\text{standard}} = \mathbb{E}_{z_t} [\text{Var}(x|z_t)] = \mathbb{E}_{z_t} [\mathbb{E}_x [\|x - \mathbb{E}[x|z_t]\|_2^2 | z_t]]. \quad (13)$$

Because the unconstrained pixel manifold is highly entangled, diverse target images map to the same noisy state  $z_t$ , making  $\text{Var}(x|z_t)$  exceptionally large. This manifests empirically as *trajectory conflict*. With oracle semantic conditioning, the Bayes-optimal predictor becomes  $\mathbb{E}[x|z_t, s_0]$ , and its irreducible uncertainty is bounded by:

$$\mathcal{E}_{\text{oracle}} = \mathbb{E}_{z_t, s_0} [\text{Var}(x|z_t, s_0)]. \quad (14)$$

As initially introduced in Equation 5, the total uncertainty in the unconstrained generation can be decomposed according to the Law of Total Variance:

$$\text{Var}(x|z_t) = \mathbb{E}_{s_0|z_t} [\text{Var}(x|z_t, s_0)] + \text{Var}_{s_0|z_t} (\mathbb{E}[x|z_t, s_0]). \quad (15)$$

By taking the expectation over  $z_t$  on both sides, we obtain the relationship between the optimization burdens of the two paradigms:

$$\mathbb{E}_{z_t} [\text{Var}(x|z_t)] = \mathbb{E}_{z_t, s_0} [\text{Var}(x|z_t, s_0)] + \mathbb{E}_{z_t} [\text{Var}_{s_0|z_t}(\mathbb{E}[x|z_t, s_0])]. \quad (16)$$

Since variance is a strictly non-negative quantity, Equation 16 mathematically guarantees the search space contraction under the oracle condition:

$$\mathcal{E}_{\text{oracle}} \leq \mathcal{E}_{\text{standard}}. \quad (17)$$

Therefore, oracle semantic conditioning reduces the Bayes ambiguity of the optimal transport problem. Motivated by this decomposition, our decoupled architecture approximates the oracle regime by explicitly predicting the semantic constraint  $\hat{s}_0$ . As corroborated by VA-VAE [42], mapping an isotropic noise prior to a low-dimensional discriminative latent space is easier than a non-discriminative counterpart. Conditioned on this stable prediction, the primary Pixel Space Generator only needs to resolve the substantially reduced residual variance. While not a formal guarantee, this provides a theoretical explanation for how semantic waypoints structurally shrink the generative search space and untangle overlapping trajectories.

While Equation 16 characterizes ambiguity in terms of conditional variance, directly estimating  $\text{Var}(x|z_t)$  in high-dimensional image space is empirically impractical. Accurately computing this quantity requires repeated samples from nearly identical continuous noisy states  $z_t$ , which is severely hindered by the curse of dimensionality, as well as the handling of an astronomically large conditional covariance matrix. We therefore adopt two inference-time proxies that reflect the directional disagreement and guidance sensitivity of the learned vector field. Following standard  $v$ -prediction formulations, the estimated velocity at integration timestep  $t$  is defined as:

$$\hat{v} = \frac{\hat{x} - z_t}{\max(1 - t, \tau_{\text{eps}})}. \quad (18)$$

During Classifier-Free Guidance (CFG), the conditional and unconditional velocities are extrapolated using a guidance scale  $w$ :

$$\hat{v}_{\text{cfg}} = \hat{v}_{\text{uncond}} + w(\hat{v}_{\text{cond}} - \hat{v}_{\text{uncond}}). \quad (19)$$

To quantify the degree of conflict, we introduce two sample-level metrics measured continuously across the integration steps:

- *Pairwise Directional Conflict*: This measures the geometric opposition between the vector field conditioned on the target label  $y$  and an alternative counterfactual label  $y_{\text{alt}}$ . We compute the cosine distance:

$$\mathcal{C}_{\text{pair}}(t) = 0.5 \cdot (1 - \cos(\hat{v}_{\text{cond}}, \hat{v}_{\text{alt}})). \quad (20)$$

Higher values indicate severe gradient interference, where paths destined for different semantic endpoints spatially overlap and pull the trajectory in contradictory directions.

**Table 4:** Quantitative comparison of trajectory conflict between JiT [22] and WiT.

| Metric                 | Position                     | JiT [22] | WiT      | Difference                       |
|------------------------|------------------------------|----------|----------|----------------------------------|
| Pairwise Conflict      | Midpoint ( $t \approx 0.5$ ) | 1.294e-4 | 8.363e-5 | <b>1.55</b> $\times$ more stable |
| Pairwise Conflict      | Maximum Peak                 | 8.532e-3 | 5.262e-3 | <b>1.62</b> $\times$ more stable |
| CFG Rel $L_2$ Distance | Midpoint ( $t \approx 0.5$ ) | 1.304e-2 | 1.159e-2 | <b>1.13</b> $\times$ more stable |

- *CFG Relative  $L_2$  Distance*: This measures the magnitude of divergence between the conditional and unconditional vector fields:

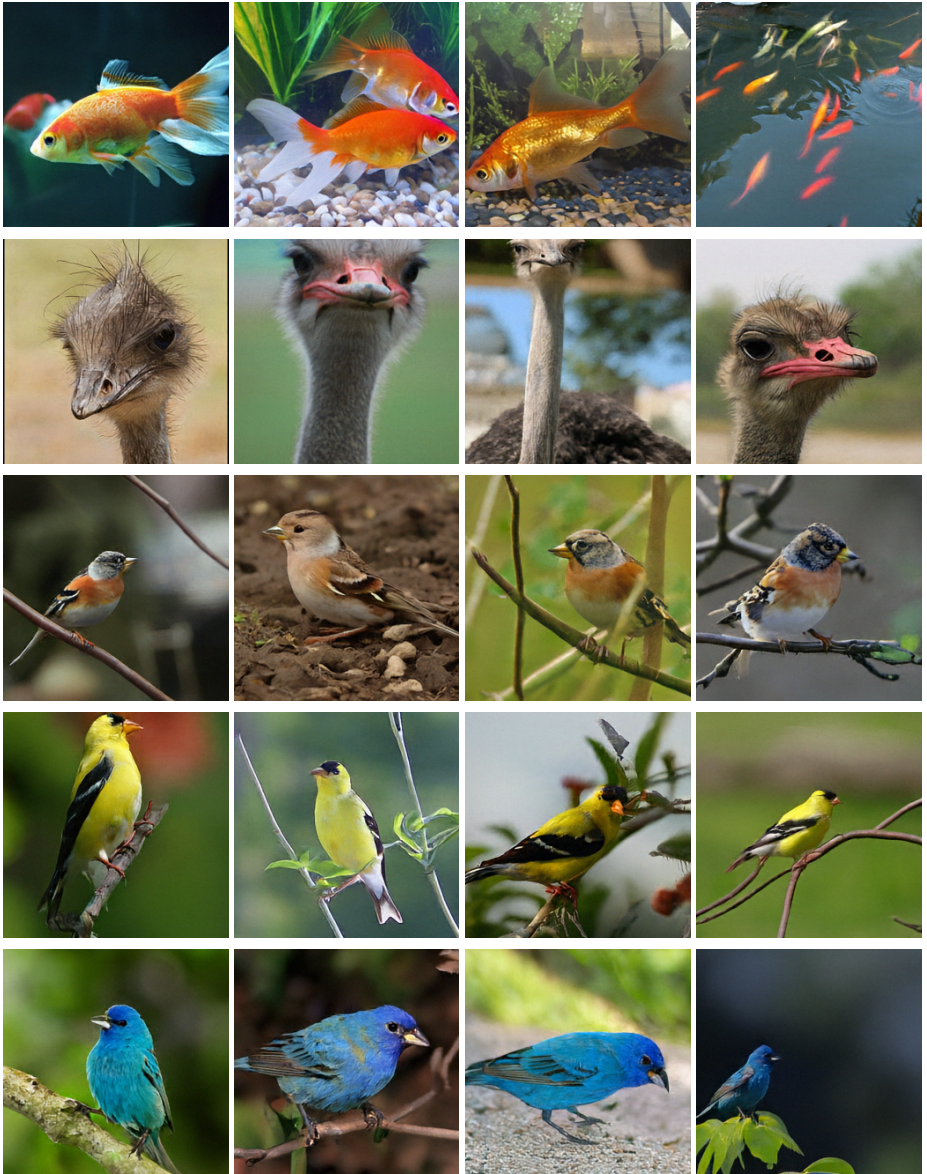
$$C_{\text{rel}}(t) = \frac{\|\hat{v}_{\text{cond}} - \hat{v}_{\text{uncond}}\|_2}{\|\hat{v}_{\text{cond}}\|_2}. \quad (21)$$

We evaluate these metrics over the course of the full generation trajectory using a 50-step Heun solver. For each integration step  $t_i$ , we compute  $\hat{v}_{\text{cond}}$ ,  $\hat{v}_{\text{uncond}}$ , and  $\hat{v}_{\text{alt}}$ , where the counterfactual label is defined as  $y_{\text{alt}} = (y + \text{stride}) \bmod C$ , with  $C$  representing the total number of classes. The metrics are averaged across multiple batches to yield stable trajectory curves over  $t \in [0, 1]$ . We compare our proposed WiT against the direct pixel-space baseline, JiT [22].

Table 4 summarizes the trajectory conflict metrics at critical points during the generative flow: the integration midpoint (where  $t \approx 0.5$ ) and the maximum peak conflict observed across the entire timeline. As demonstrated in Table 4, standard pixel-space Flow Matching (like JiT [22]) suffers from overlapping trajectories. By successfully anchoring the generation trajectories to low-dimensional semantic waypoints, WiT structurally untangles these paths, demonstrating approximately  $1.62\times$  *higher stability* in pairwise conflict at the peak integration phase. This validates our theoretical framework: satisfying the explicit semantic constraint narrows the search space, yielding a smoother, highly separable vector field and robust visual structural integrity.

## 6 Conclusion

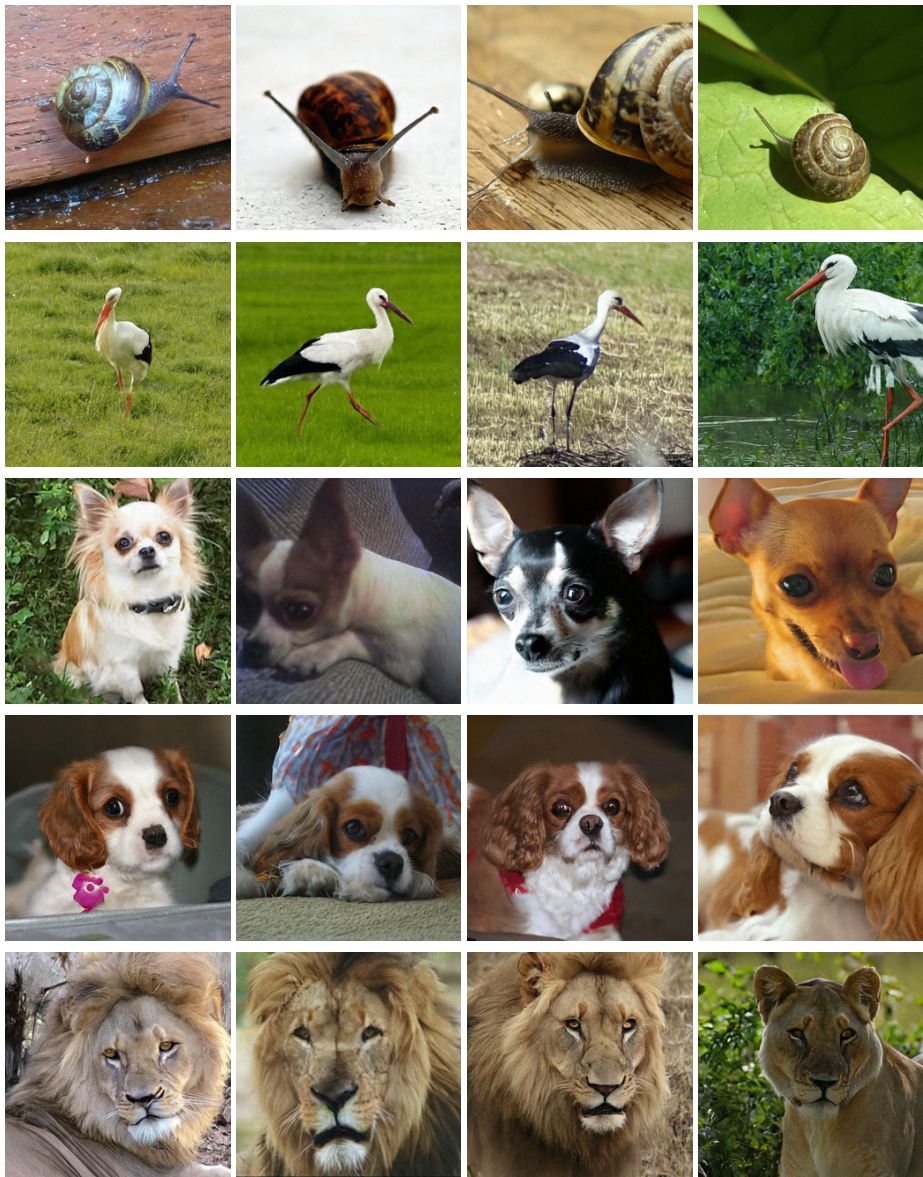
In this paper, we presented Waypoint Diffusion Transformers (WiT), a novel generative paradigm designed to resolve the severe trajectory conflict inherent in pixel-space Flow Matching. Recognizing that the raw pixel manifold is naturally entangled and resistant to direct regularization, we explicitly decoupled the generative process into semantic navigation and high-realistic texture synthesis. By projecting the discriminative feature space of pre-trained vision models into compact semantic waypoints, WiT successfully factors the complex noise-to-pixel optimal transport path. During integration, a lightweight Waypoints Generator dynamically infers these structural anchors, which subsequently provide spatially-varying guidance to the primary diffusion transformer via our proposed Just-Pixel AdaLN mechanism. Extensive experiments on ImageNet  $256 \times 256$  demonstrate that WiT achieves a state-of-the-art performance among pure pixel-space architectures, surpassing even heavy VAE-compressed latent models, while delivering a remarkable  $2.2\times$  training speedup over JiT [22].



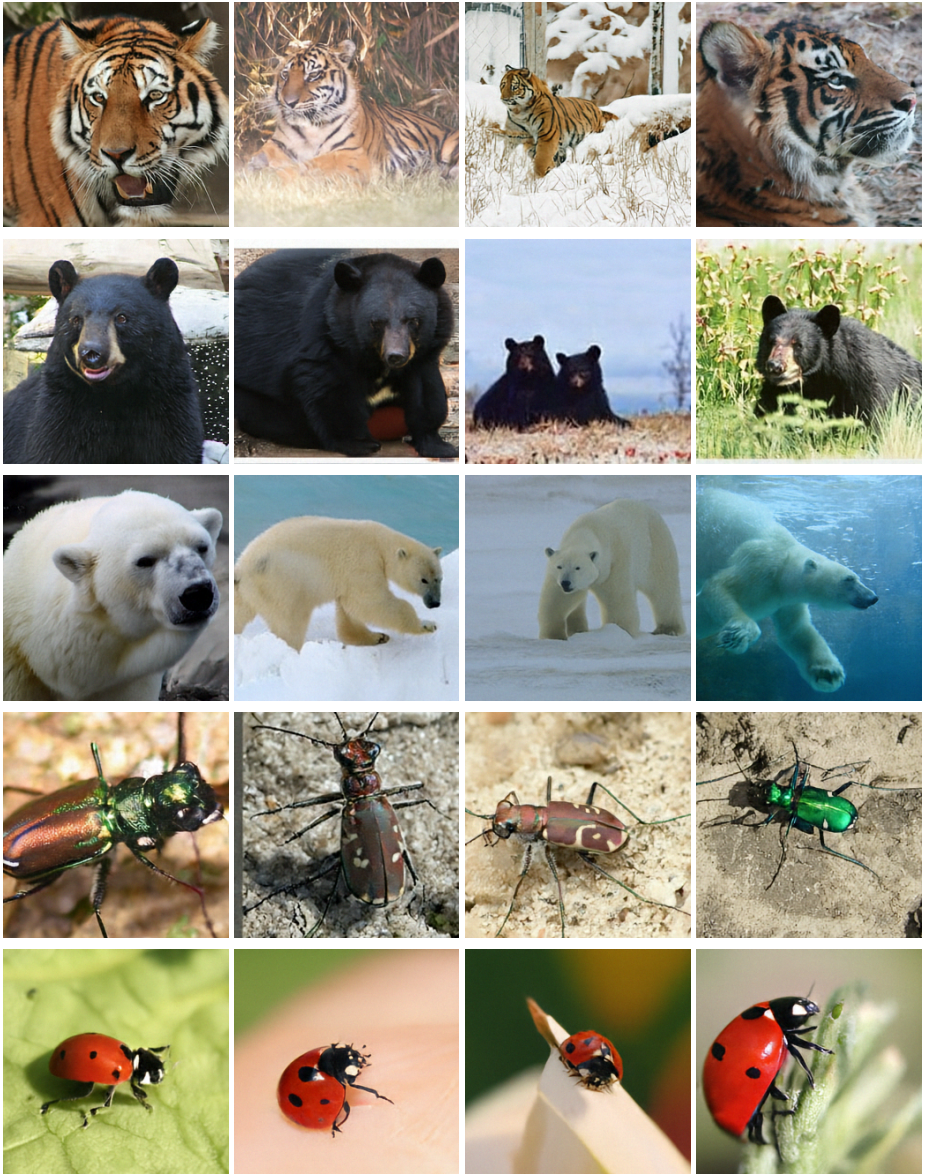
**Fig. 6:** Visual Results of WiT-XL/16 on ImageNet  $256 \times 256$  [7].



Fig. 7: Visual Results of WiT-XL/16 on ImageNet  $256 \times 256$  [7].



**Fig. 8:** Visual Results of WiT-XL/16 on ImageNet  $256 \times 256$  [7].



**Fig. 9:** Visual Results of WiT-XL/16 on ImageNet  $256 \times 256$  [7].

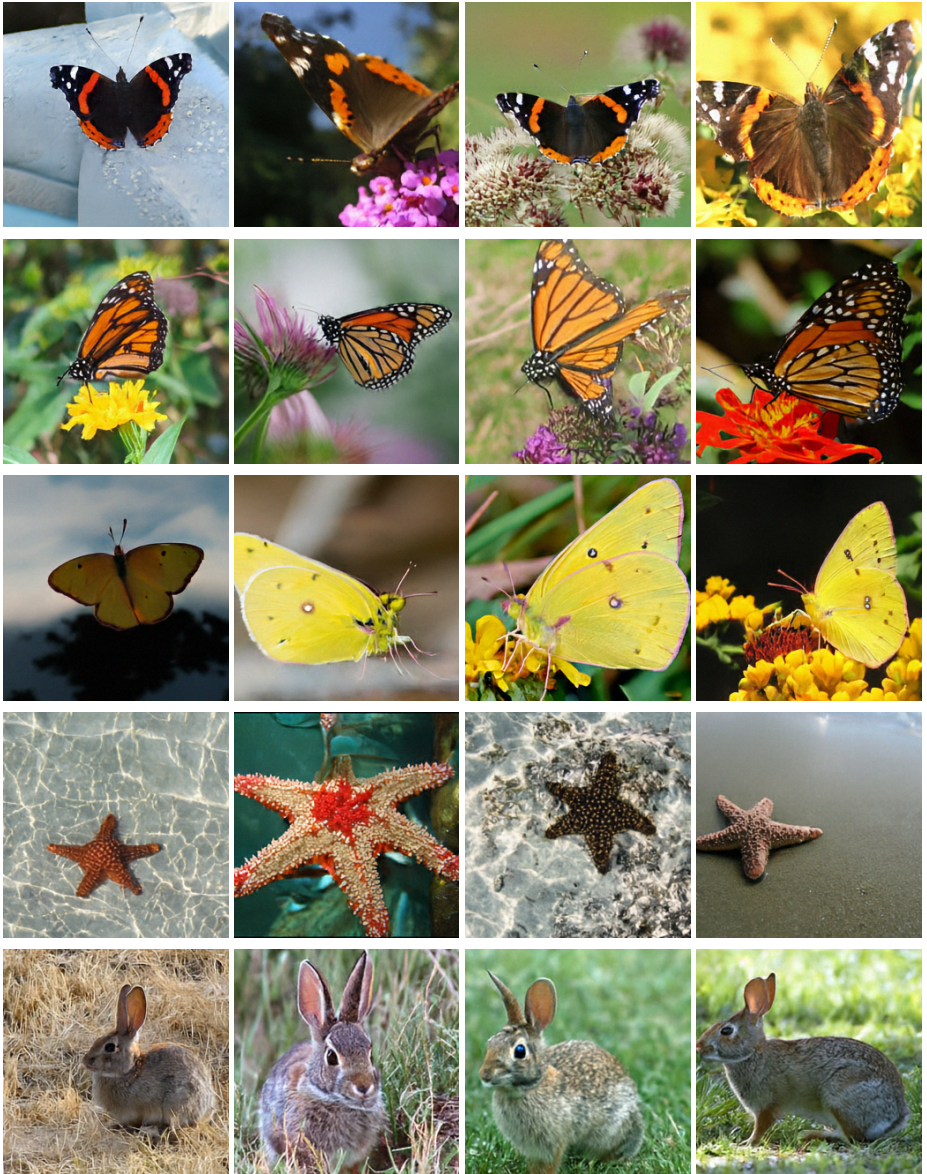


**Fig. 10:** Visual Results of WiT-XL/16 on ImageNet  $256 \times 256$  [7].

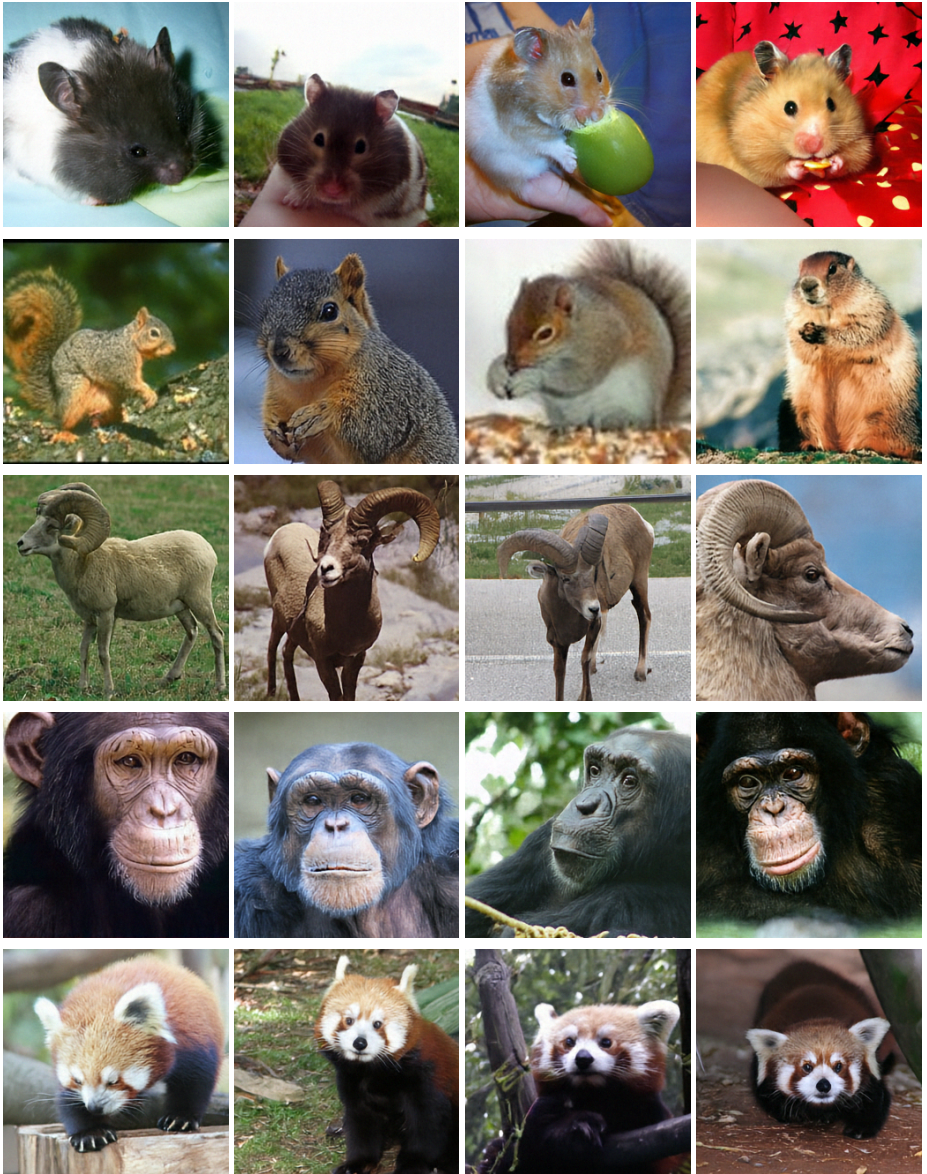


**Fig. 11:** Visual Results of WiT-XL/16 on ImageNet  $256 \times 256$  [7].

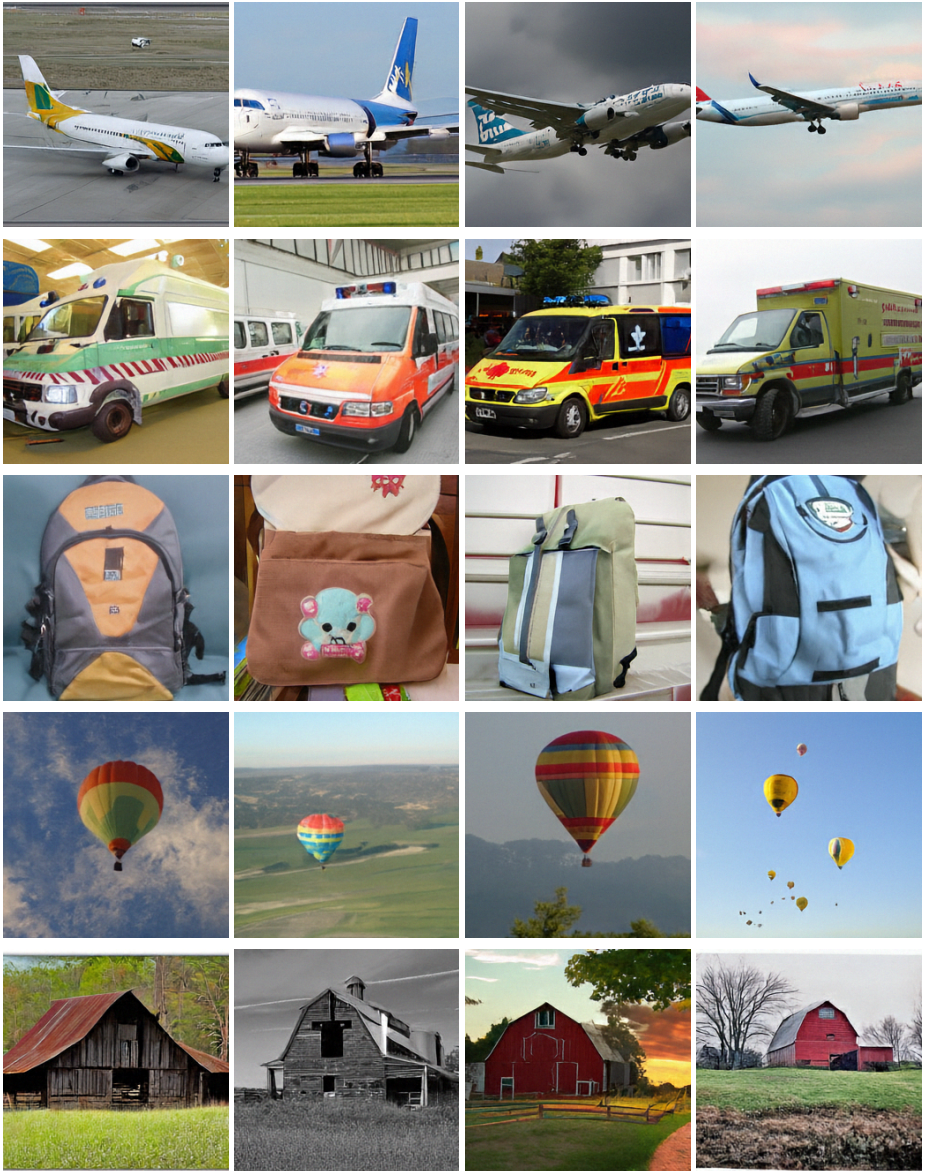
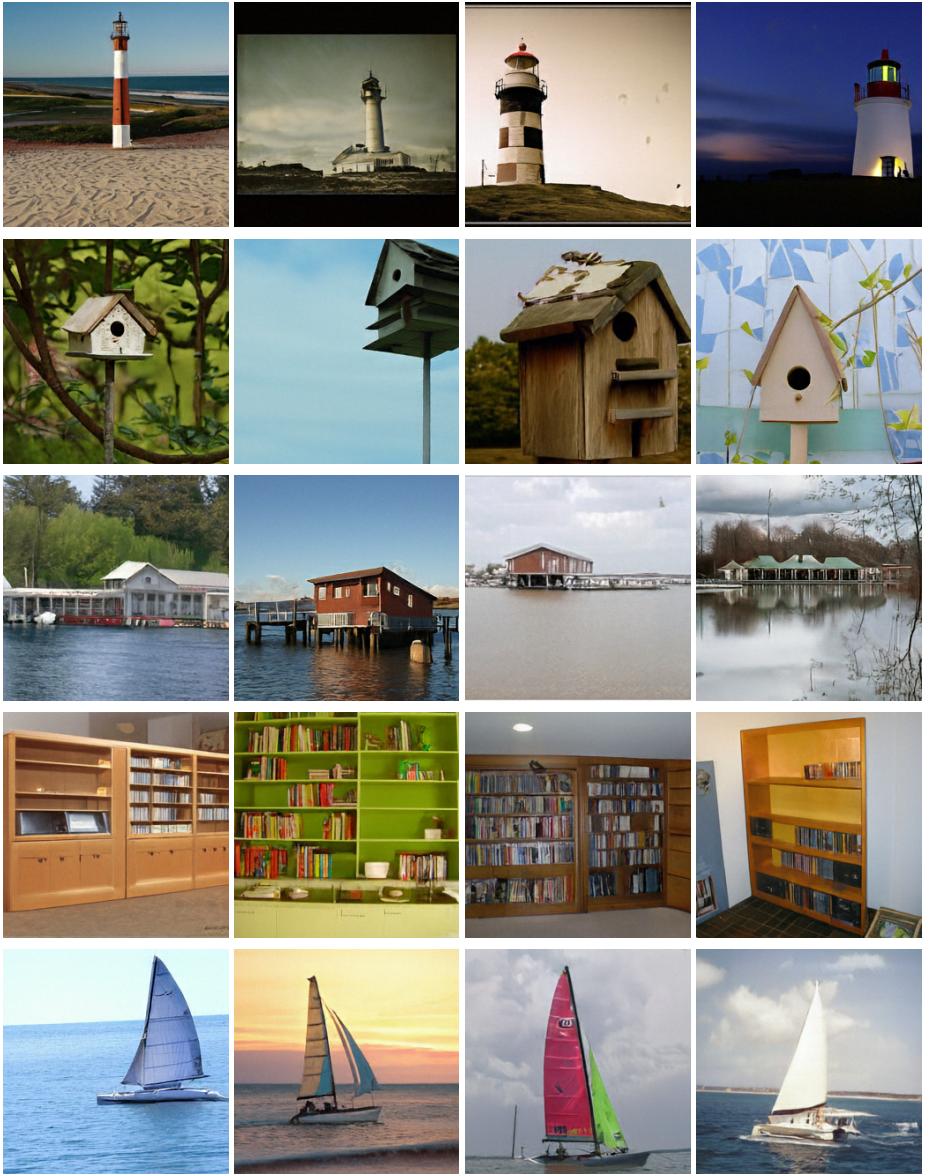


Fig. 12: Visual Results of WiT-XL/16 on ImageNet  $256 \times 256$  [7].



**Fig. 13:** Visual Results of WiT-XL/16 on ImageNet  $256 \times 256$  [7].

## Acknowledgements

We would like to thank Qiming Hu for the insightful discussions and feedback. The computational resources of this work was partially supported by TPU Research Cloud (TRC).

## References

1. Albergo, M.S., Vanden-Eijnden, E.: Building normalizing flows with stochastic interpolants. In: ICLR (2023)
2. Baade, A., Chan, E.R., Sargent, K., Chen, C., Johnson, J., Adeli, E., Fei-Fei, L.: Latent forcing: Reordering the diffusion trajectory for pixel-space image generation. arXiv preprint arXiv:2602.11401 (2026)
3. Black Forest Labs: FLUX.2: Analyzing and enhancing the latent space of FLUX – representation comparison (2025), <https://bfl.ai/research/representation-comparison>
4. Blattmann, A., Dockhorn, T., Kulal, S., Mendelevitch, D., Kilian, M., Lorenz, D., Levi, Y., English, Z., Voleti, V., Letts, A., et al.: Stable video diffusion: Scaling latent video diffusion models to large datasets. arXiv:2311.15127 (2023)
5. Chen, S., Ge, C., Zhang, S., Sun, P., Luo, P.: PixelFlow: Pixel-space generative models with flow. arXiv:2504.07963 (2025)
6. Chen, Z., Zhu, J., Chen, X., Zhang, J., Hu, X., Zhao, H., Wang, C., Yang, J., Tai, Y.: Dip: Taming diffusion models in pixel space. arXiv preprint arXiv:2511.18822 (2025)
7. Deng, J., Dong, W., Socher, R., Li, L.J., Li, K., Fei-Fei, L.: ImageNet: A large-scale hierarchical image database. In: CVPR (2009)
8. Dhariwal, P., Nichol, A.: Diffusion models beat GANs on image synthesis (2021)
9. Dinh, L., Sohl-Dickstein, J., Bengio, S.: Density estimation using real nvp. In: International Conference on Learning Representations (2017)
10. Esser, P., Rombach, R., Ommer, B.: Taming Transformers for high-resolution image synthesis. In: CVPR (2021)
11. Goodfellow, I., Pouget-Abadie, J., Mirza, M., Xu, B., Warde-Farley, D., Ozair, S., Courville, A., Bengio, Y.: Generative adversarial networks. *Communications of the ACM* **63**(11), 139–144 (2020)
12. Ho, J., Jain, A., Abbeel, P.: Denoising diffusion probabilistic models (2020)
13. Ho, J., Salimans, T.: Classifier-free diffusion guidance. In: NeurIPS Workshops (2021)
14. Hoogeboom, E., Heek, J., Salimans, T.: simple diffusion: End-to-end diffusion for high resolution images. ICML (2023)
15. Hoogeboom, E., Mensink, T., Heek, J., Lamerigts, K., Gao, R., Salimans, T.: Simpler Diffusion (SiD2): 1.5 FID on ImageNet512 with pixel-space diffusion. In: CVPR (2025)
16. Jabri, A., Fleet, D., Chen, T.: Scalable adaptive computation for iterative generation. In: ICML (2023)
17. Kingma, D.P., Dhariwal, P.: Glow: Generative flow with invertible 1x1 convolutions. In: Advances in neural information processing systems (2018)
18. Kynkäänniemi, T., Aittala, M., Karras, T., Laine, S., Aila, T., Lehtinen, J.: Applying guidance in a limited interval improves sample and distribution quality in diffusion models (2024)

19. Lei, J., Liu, K., Berner, J., Yu, H., Zheng, H., Wu, J., Chu, X.: Advancing end-to-end pixel space generative modeling via self-supervised pre-training. arXiv:2510.12586 (2025)
20. Leng, X., Singh, J., Hou, Y., Xing, Z., Xie, S., Zheng, L.: Repa-e: Unlocking vae for end-to-end tuning with latent diffusion transformers. arXiv preprint arXiv:2504.10483 (2025)
21. Leng, X., Singh, J., Murdock, R., Smith, E., Li, R., Hou, Y., Xing, Z., Xie, S., Zheng, L.: Family of end-to-end tuned vae for supercharging t2i diffusion transformers. <https://end2end-diffusion.github.io/repae-t2i/> (2025)
22. Li, T., He, K.: Back to basics: Let denoising generative models denoise. arXiv preprint arXiv:2511.13720 (2025)
23. Li, T., Sun, Q., Fan, L., He, K.: Fractal generative models. arXiv:2502.17437 (2025)
24. Lipman, Y., Chen, R.T.Q., Ben-Hamu, H., Nickel, M., Le, M.: Flow matching for generative modeling. In: ICLR (2023)
25. Liu, X., Gong, C., Liu, Q.: Flow straight and fast: Learning to generate and transfer data with rectified flow. In: ICLR (2023)
26. Ma, N., Goldstein, M., Albergo, M.S., Boffi, N.M., Vanden-Eijnden, E., Xie, S.: SiT: Exploring flow and diffusion-based generative models with scalable interpolant Transformers. In: ECCV (2024)
27. Ma, Z., Wei, L., Wang, S., Zhang, S., Tian, Q.: Deco: Frequency-decoupled pixel diffusion for end-to-end image generation. arXiv preprint arXiv:2511.19365 (2025)
28. Mentzer, F., Minnen, D., Agustsson, E., Tschannen, M.: Finite scalar quantization: VQ-VAE made simple. In: ICLR (2024)
29. Oquab, M., Darcet, T., Moutakanni, T., Vo, H.V., Szafraniec, M., Khalidov, V., Fernandez, P., Haziza, D., Massa, F., El-Nouby, A., Howes, R., Huang, P.Y., Xu, H., Sharma, V., Li, S.W., Galuba, W., Rabbat, M., Assran, M., Ballas, N., Synnaeve, G., Misra, I., Jegou, H., Mairal, J., Labatut, P., Joulin, A., Bojanowski, P.: Dinov2: Learning robust visual features without supervision (2023)
30. Peebles, W., Xie, S.: Scalable diffusion models with Transformers. In: ICCV (2023)
31. Rombach, R., Blattmann, A., Lorenz, D., Esser, P., Ommer, B.: High-resolution image synthesis with latent diffusion models. In: CVPR (2022)
32. Salimans, T., Ho, J.: Progressive distillation for fast sampling of diffusion models. In: ICLR (2022)
33. Sauer, A., Schwarz, K., Geiger, A.: StyleGAN-XL: Scaling StyleGAN to large diverse datasets. In: SIGGRAPH (2022)
34. Shi, M., Wang, H., Zheng, W., Yuan, Z., Wu, X., Wang, X., Wan, P., Zhou, J., Lu, J.: Latent diffusion model without variational autoencoder. arXiv:2510.15301 (2025)
35. Siméoni, O., Vo, H.V., Seitzer, M., Baldassarre, F., Oquab, M., Jose, C., Khalidov, V., Szafraniec, M., Yi, S., Ramamonjisoa, M., Massa, F., Haziza, D., Wehrstedt, L., Wang, J., Darcet, T., Moutakanni, T., Sentana, L., Roberts, C., Vedaldi, A., Tolan, J., Brandt, J., Couprie, C., Mairal, J., Jégou, H., Labatut, P., Bojanowski, P.: DINOv3 (2025), <https://arxiv.org/abs/2508.10104>
36. Singh, J., Leng, X., Wu, Z., Zheng, L., Zhang, R., Shechtman, E., Xie, S.: What matters for representation alignment: Global information or spatial structure? arXiv preprint arXiv:2512.10794 (2025)
37. Song, Y., Sohl-Dickstein, J., Kingma, D.P., Kumar, A., Ermon, S., Poole, B.: Score-based generative modeling through stochastic differential equations. In: ICLR (2021)

38. Tong, A., FATRAS, K., Malkin, N., Huguet, G., Zhang, Y., Rector-Brooks, J., Wolf, G., Bengio, Y.: Improving and generalizing flow-based generative models with minibatch optimal transport. *Transactions on Machine Learning Research* (2024), <https://openreview.net/forum?id=CD9Snc73AW>, expert Certification
39. Tschannen, M., Pinto, A.S., Kolesnikov, A.: JetFormer: an autoregressive generative model of raw images and text. In: *ICLR* (2025)
40. Wang, S., Gao, Z., Zhu, C., Huang, W., Wang, L.: PixNerd: Pixel neural field diffusion. *arXiv:2507.23268* (2025)
41. Wang, S., Tian, Z., Huang, W., Wang, L.: DDT: Decoupled diffusion Transformer. *arXiv:2504.05741* (2025)
42. Yao, J., Yang, B., Wang, X.: Reconstruction vs. generation: Taming optimization dilemma in latent diffusion models. In: *CVPR* (2025)
43. Yu, S., Kwak, S., Jang, H., Jeong, J., Huang, J., Shin, J., Xie, S.: Representation alignment for generation: Training diffusion Transformers is easier than you think. In: *ICLR* (2025)
44. Yu, Y., Xiong, W., Nie, W., Sheng, Y., Liu, S., Luo, J.: Pixeldit: Pixel diffusion transformers for image generation. *arXiv preprint arXiv:2511.20645* (2025)
45. Zheng, B., Ma, N., Tong, S., Xie, S.: Diffusion Transformers with representation autoencoders. *arXiv:2510.11690* (2025)